Desalination and Water Treatment
www.deswater.com
doi: 10.5004/dwt.2020.24869

174 (2020) 215–229
January

Catalytic ozonation assisted by rGO/C-MgO in the degradation of humic acid from aqueous solution: modeling and optimization by response surface methodology, kinetic study

Ghorban Asgari[a], Abdolmotaleb Seidmohammadi[a], Mehdi Salari[a,*], Bahman Ramavandi[b], Javad Faradmal[c]

[a]*Social Determinants of Health Research Center (SDHRC), Department of Environmental Health Engineering, School of Public Health, Hamadan University of Medical Science, Hamadan, Iran, emails: Msalari_22@yahoo.com (M. Salari), asgari@umsha.ac.ir (G. Asgari), motalebsm@gmail.com (A. Seidmohammadi)*
[b]*Department of Environmental Health Engineering, School of Public Health, Bushehr University of Medical Sciences, Bushehr, Iran, email: ramavandi@bpums.ac.i*
[c]*Department of Biostatistics and Epidemiology, School of Public Health, Hamadan University of Medical Science, Hamadan, Iran, email: javad.faradmal@umsha.ac.ir*

Received 23 April 2019; Accepted 8 September 2019

ABSTRACT

The present study investigated the performance of catalytic ozonation with C-MgO-doped reduced graphene oxide support (rGO/C-MgO) in humic acid (HA) removal from aqueous solution in a lab-scale batch reactor. The analyses of scanning electron microscope, energy dispersive X-ray spectroscopy, X-ray diffraction, UV-Vis, and Brunauer–Emmett–Teller showed that the rGO/C-MgO has been synthesized successfully. Photoluminescence analysis confirmed that the number of oxygen vacancy defect in C-MgO structure increased strongly rather than MgO because of the presence of carbon in the structure of MgO. Response surface methodology-central composite design (RSM-CCD) suggested a quadratic polynomial model (F-value = 363.38 and R^2 = 0.9971) for describing the effects of independent variables on the response (removal efficiency). The optimum values of the independent parameters based on the maximum removal efficiency were obtained at pH = 8.46, contact time = 12 min, catalyst dose = 1 g/L and NaCl = 10 mg/L. The salicylic acid and chloroform application as radical scavengers in the reaction solution demonstrated that non-hydroxyl radical mechanisms are the main reactions involved in HA degradation. Synergetic effect exhibits a noticeable enhancement in the hybrid catalytic ozonation process in comparison with the separate processes. The behavior of HA degradation under the process was described as well by pseudo-first-order kinetic model with a rate constant of 0.2092 min^{-1}. The efficiency of total organic carbon removal was determined to be 86.8% and 25.3% at 100 and 10 min reaction times. In conclusion, the rGO/C-MgO composite can be suggested as a promising catalyst in catalytic ozonation process for treating water polluted with organic compounds such as HA.

Keywords: Catalytic ozonation process; rGO/C-MgO; Humic acid; Mineralization; Water treatment

1. Introduction

Humic acid (HA) is a natural organic matter produced during the degradation of the plant, algal, and microbial material [1]. Carbon, oxygen, hydrogen are the main elements of this compound, whereas other elements, such as nitrogen, phosphorous, and sulfur, can exist in small amounts in the structure of HA. The most common chemical functional

* Corresponding author.

groups in the structure of the substance are carboxyl, phenolic, carbonyl, and hydroxyl, which are mainly connected to aliphatic or aromatic carbons [2].

Raw surface waters may have high levels of HA, which can affect adversely the performance of common treatment processes such as coagulation process. On the other hand, during chlorination of raw water contaminated with a high density of HA, disinfectant by-products are formed that are toxic to human beings [3]. Therefore, it is necessary to effectively eliminate HA from raw waters prior to chlorination. Additionally, the presence of high concentrations of HA in treated water causes color and odor changes, and the growth of bacteria in drinking water distribution systems [4]. Regarding the above challenges and concerns, it is essential to further research about new efficient treatment processes to resolve the above problems by the effective removal of HA. In practical conditions, the presence of salts, such as NaCl is likely to affect the efficiency of the processes employed in water treatment; nevertheless, this effect is not elucidated. Thus, it seems critical to investigate the influence of NaCl presence in HA removal from water during a treatment process.

To date, some conventional methods, such as advanced oxidation [5, 6], membrane filtration [7], biofiltration [8], coagulation precipitation [9], ion exchange [10], and adsorption [11] have been widely studied for the removal of HA material from water. Ozone is well known as a potent oxidant with good efficiency in the degradation of organic matters [12]. However, single ozonation process is considered as an expensive method owing to its high production cost; especially if it is used in large-scale applications [13]. In recent years, catalytic ozonation process has been introduced as a new class of advanced oxidation processes (AOPs). In a catalytic ozonation process, ozone and a solid compound (as a catalyst) react together to generate powerful oxidizing radicals, such as hydroxyl radicals ($OH^{\bullet}$). The $OH^{\bullet}$ is a non-selective oxidizing species with greater oxidation potential (E^0: 2.80 eV) relative to conventional oxidants such as molecular ozone (E^0 = 2.07 eV) [14]. The catalytic ozonation has been extensively investigated as a novel AOP due to its high efficiency in the degradation and mineralization of refractory organic compounds at a high oxidation rate and low reaction time [15]. A wide variety of metal oxides or supported metal oxides, such as Fe_2O_3, ZnO, TiO_2, MnO_2, Al_2O_3, Fe^{2+}, Au/TiO_2, WO_3-TiO_2, and some porous materials (e.g., carbon materials, activated carbon, or zeolite), have been evaluated so far to reveal their catalytic capacity in the catalytic ozonation process involved in water and wastewater treatment [15,16]. Among them, activated carbon, MnO_2, and Fe_2O_3 have appeared to be more capable in the catalytic ozonation process; however, each of them is faced with specific problems such as low mechanical strength of activated carbon, easily leaching of MnO_2, and the need to the improvement of catalytic activity of Fe_2O_3 [17]. Therefore, more research efforts are necessary to develop new efficient catalysts. MgO, because of some promising features including high stability in water, high surface activity, and reactivity, non-toxicity and being environmentally friendly, has been paid great attention to be used as a catalyst in the catalytic ozonation process [18]. So far, the catalytic ozonation assisted with MgO has been evaluated for the removal of several refractory organic compounds, such as dyes [19], phenol [20], 4-chlorophenol [17], and formaldehyde [21], and related results confirm the noticeable catalytic capacity of MgO.

The agglomeration and subsequent decline of the specific surface area of catalysts caused during calcination of their precursor raise concerns for the reduction of catalytic activity. Currently, it is reported that by calcination of MgO in the presence of sucrose as carbon source and subsequent addition of a carbon element into MgO structure (donated as C-MgO), the agglomeration of the catalyst can be potentially prevented, and catalytic capacity and adsorbing properties of MgO obviously obtain improvement [22]. Additionally, it has been found that metal oxides such as TiO_2 modified by means of non-metal elements (e.g., N (nitrogen), F (Fluorine), S (sulfur), and C (carbon) have higher catalytic and photocatalytic activity due to increase of surface defects as a result of oxygen vacancies [23–26]. Moussavi et al. [23] reported that S element by increasingly creating oxygen vacancy defects into MgO structure promotes the catalytic properties of S-MgO.

The small size of nano-catalysts makes their separation from a reaction solution very difficult. Nowadays, researchers have proposed different materials, such as pumice, zeolite, silica gel, and alumina, as a carrier or support to grow various nanoparticles and to easily separate catalysts [27]. Reduced graphene oxide (rGO) as a support for a catalyst has been applied due to its excellent features such as surface functional groups, defective structures and textural properties, which can effectively influence the efficiency of ozonation and photocatalytic processes [28]. On the other hand, the enrichment of pollutant molecules around the rGO surface and the easily recyclable of a catalyst doped on rGO surface can be considered as the other attractive merits of rGO application in the role of support for a catalyst [29]. In the study of Feng et al. [30], it was reported that rGO promotes oxygen vacancies in the structure of perovskite compound. As a result, it can be deduced that using rGO as support can increase the number of oxygen vacancy defect in the structure of C-MgO composite.

Traditionally, optimization of a process in analytical chemistry is conducted through monitoring of the effect of one factor at a time, while other factors are kept at fixed levels. There are major disadvantages with this technique, including lack of attention to interactive effects, need of high number of experiments to carry out the research, which subsequently leads to an increase in time, costs, and reagents and materials necessary for performing experiments [31]. To circumvent the problems, multivariate statistic techniques have been widely developed for optimizing the analytical procedures. Response surface methodology (RSM) is considered among the most popular multivariate techniques for analytical procedures [22]. In RSM approach, central composite design (CCD) is known as one of the most frequently used response surface designs. Nowadays, CCD-RSM technique is widely used in water and wastewater treatment processes, because it reduces the experimental costs and time by minimizing the number of experiments required and can determine and optimize the quadratic and interaction effects of independent parameters beside their linear effects [32].

This study was aimed to study the catalytic ozonation with C-MgO doped on reduced graphene oxide (C-MgO/rGO) in the removal of HA from aqueous solutions. In this research

work, the effects of pH, NaCl concentration, catalyst dosage, and reaction time variables on the performance of the catalytic ozonation process were studied first. Optimization and modeling of effects of the operational parameters on the catalytic ozonation in HA removal were performed by using CCD-RSM approach. Lastly, the mechanism of HA degradation, synergistic effect and the reusability of the rGO-C/MgO were studied under this research.

2. Materials and methods

2.1. Materials

Graphite powder (average size of nearly 20 μm and molecular weight of 12.01), HA, 35 wt% hydrazine solution, and 28 wt% ammonia solution were purchased from Sigma-Aldrich Co., Germany. Magnesium nitrate hexahydrate ($MgNO_3{\cdot}6H_2O$), sulfuric acid (H_2SO_4, 0.1 N), hydrochloric acid (HCl, 0.1 N), sodium hydroxide (NaOH, 1 N), hydrogen peroxide 30 v/v% (H_2O_2), sodium nitrate ($NaNO_3$), and potassium permanganate ($KMnO_4$) were supplied from Merck Co., Germany. All the used chemicals were of analytical grade and used without further purification.

2.2. Synthesis of graphene oxide (GO)

The modified Hummers' method was employed to synthesize graphene oxide (GO) applied as a precursor to prepare rGO [33]. Briefly, 2 g graphite powder and 1 g $NaNO_3$ were dissolved in a 250 mL flask having 50 mL concentrated H_2SO_4, and the obtained solution was kept under stirring for 2 h. In the following, 150 mL deionized water, 7 mL H_2O_2, and 7.3 g $KMnO_4$ were added to the solution under vigorous stirring and the temperature of below 10°C. After that, the suspension was centrifuged to obtain yellow-brown graphite oxide. The resultant sample was then washed several times with deionized water and diluted HCl (3 wt%), and finally dried in a vacuum oven at 50°C for 24 h. The resultant exfoliated GO was placed under ultrasound irradiation for 3 h to be dispersed in 200 mL deionized water and then dried at 60°C for 24 h after being centrifuged at 4,500 rpm for 15 min [34].

2.3. Synthesis of reduced graphene oxide (rGO)

To synthesize rGO, 1 g of the synthesized GO with 25 μL hydrazine solution and 175 μL ammonia solution was dissolved in 25 mL deionized water, and the obtained mixture was mixed at 500 rpm velocity for 1 h at 90°C in a water bath. The mixture was finally centrifuged at 7,000 rpm to separate the material denoted as rGO [35].

2.4. Synthesis of C-MgO

The sol-gel method was employed to synthesize MgO nanoparticles. The procedure was as follows: 32 g of $MgNO_3{\cdot}6H_2O$ was mixed in 200 mL of deionized water by a magnetic mixer, and then 50 mL of 1 N NaOH solution was added into the solution in continuous stirring condition. The resulted solution was mixed for 2 h to generate magnesium hydroxide ($Mg(OH)_2$), which was then separated from the solution by centrifuging the solution at 5,000 rpm for 7 min. $Mg(OH)_2$ gel was washed twice with DI water and dissolved together with sucrose powder at 1/10 w/w ratio into 200 mL deionized water for 1 h. After that, the suspension was dried at 100°C for 24 h. To produce C-MgO nanoparticles, the resulting material was calcinated at 550°C for 2 h in an electric furnace [36].

2.5. Preparation of rGO/C-MgO

The rGO-C-MgO composite was synthesized at the rGO to C-MgO ratios of 5:1, 1:1, and 1:5. According to the impregnation method, 0.6 g of the rGO was simultaneously dissolved into three beakers containing 100 mL DI water and sonicated for 60 min. Then, the calculated amounts of the C-MgO (0.12, 0.6, and 3 g) were added simultaneously into the solutions. After 30 min sonication time, the suspensions were separated from the solution by centrifuging at 5,000 rpm, and finally dried at 60°C.

2.6. Catalyst characterization

The Brunauer–Emmett–Teller (BET) analysis based on N_2 adsorption/desorption isotherm was used to measure specific surface area and total pore volume of the rGO/C-MgO, and Barrett–Joyner–Halenda (BJH) method was applied to calculate pore size distribution (Micromeritics/Gemini-2372 surface area analyzer, Japan, 77 K adsorption temperature). X-ray diffraction (XRD) analysis of the GO, rGO, and rGO/C-MgO was done by Rigaku miniflex diffractometer device (Japan) in the scattering angles from 10° to 70° at 30 kV and 15 mA to evaluate crystalline phases (scanning speed of 2°/min). Scanning electron microscope (SEM) images were taken using a Hitachi S-4800 ultra-high-resolution equipment (Japan) at 12.0 kV accelerating voltage to characterize the microstructure and surface morphology of the rGO and rGO/C-MgO. Additionally, the chemical composition of the rGO/C-MgO was determined using energy dispersive X-ray spectroscopy (EDX) detector coupled to the scanning electron microscope. Photoluminescence (PL) spectrum was measured by using a Perkin-Elmer (LS55) Fluorescence spectrometer (USA) to evaluate the existence of oxygen vacancies defect in the structure of the MgO and C-MgO. Also, the UV-Vis spectra of the GO and rGO were recorded with a UV-visible spectrophotometer (model DR6000, HACH Co., USA) to assess the reduction degree. The pHzpc, at which the surface charge of rGO/C-MgO is zero was determined in accordance with the method reported elsewhere [31,37].

2.7. Experimental procedures

All experiments were conducted in a batch cylindrical glass reactor with the dimensions of 3 cm in diameter and 50 cm in depth. The inlet of ozone generator with the capacity of 1.8 mgO_3/min was connected to a pure oxygen cylinder, while the outlet was connected to the bottom of the reactor equipped with a porous diffuser for effectively dispersing ozone bubbles. For all the experiments carried out, initial HA concentration was kept constant at 30 mg/L. First, the ability of the MgO, C-MgO, and rGO in adsorption and catalytic ozonation processes were evaluated. In addition, the

catalytic capacity of three ratios of the rGO to C-MgO was examined and compared together in the catalytic ozonation. After determining the optimal ratio of the rGO to C-MgO, the parameters of pH, contact time, dosage of the rGO/C-MgO and NaCl concentration at the levels given in Table 1 were investigated in the catalytic ozonation for HA removal. Salicylic acid and chloroform were selected as radical scavengers of $OH^{\bullet}$ and $O_2^{\bullet-}$ radicals, respectively. In addition, sulfate, as anion model with relatively high affinity to occupy active sites of a catalyst was tested as an inhibitor in the catalytic ozonation. The solutions of 0.1 N H_2SO_4 and NaOH were used to adjust the solution pH. Fig. 1 shows a schematic of the experimental setup.

2.8. Experimental design

In this study, CCD-RSM technique as a statistical and mathematical approach was performed by using Design-Expert software (version 11) to quantify, model, and optimize the relationship between responses and independent variables. In this method, the number of levels of input variables studied is varied at five levels as presented in Table 1. Therefore, in the present study, the effect of rGO/C-MgO dosage, pH, reaction time, and NaCl concentration on the performance of the catalytic ozonation process in HA degradation was systematically investigated based on CCD-RSM methodology. Based on CCD method, an experimental design with 30 runs was calculated as listed in Table 2, in which 16 are related to factorial points ($\alpha = \pm 1$), 8 axial points ($\alpha = \pm 2$) and 6 replications at the center point ($\alpha = 0$).

2.9. Analytical methods

The HA concentration in the reaction solution was detected by UV-visible spectrophotometer (model DR6000, HACH Co.) at a wavelength of 254 nm. The removal efficiency of HA was determined according to Eq. (1) as follows:

Table 1
Independent variables and their levels based on central composite design

Variable	Symbol	$-\alpha$	–1	0	+1	$+\alpha$
pH	X_1	3	5	7	9	11
Contact time (min)	X_2	4	6	8	10	12
Dosage of rGO/C-MgO (g/L)	X_3	0.2	0.4	0.6	0.8	1
NaCl concentration (mg/L)	X_4	10	22.5	35	47.5	60

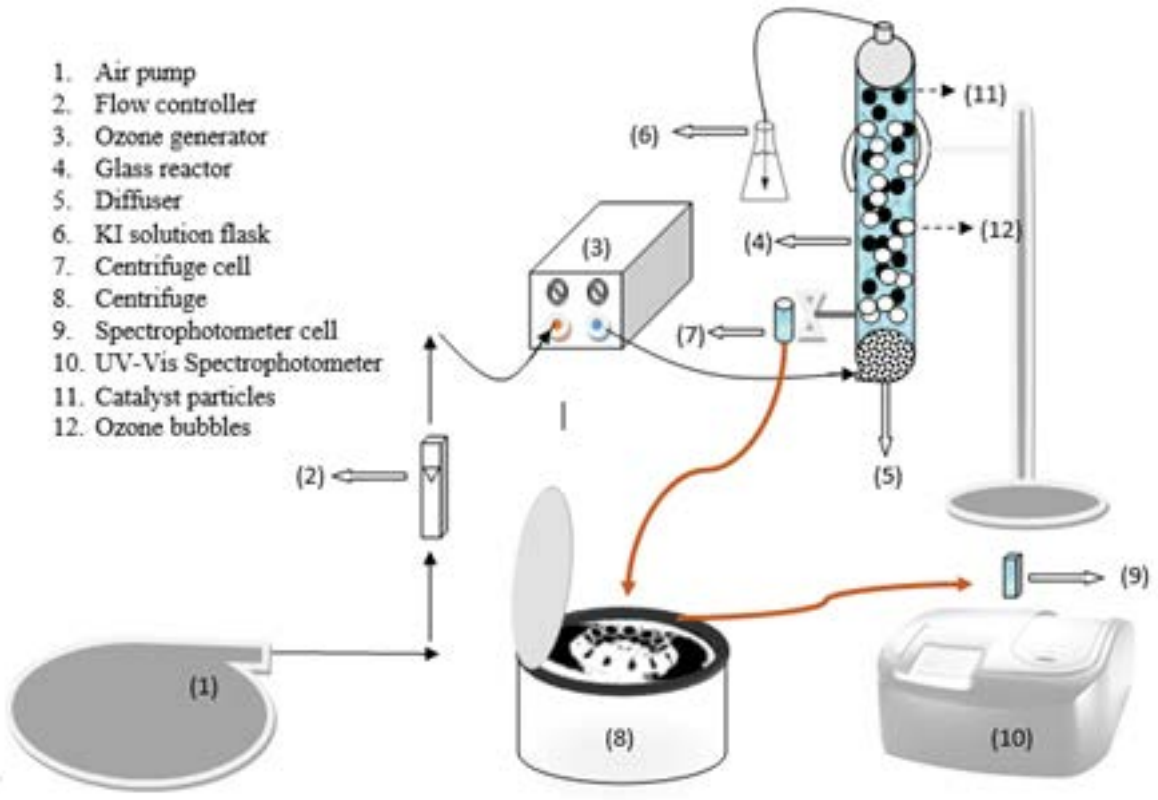

Fig. 1. Schematic of the experimental setup.

Table 2
Experimental design matrix based on central composite design; actual and predicted percentages of HA removal using the catalytic ozonation process with the rGO/C-MgO

Run order	pH	Time (min)	Catalyst dosage (g/L)	NaCl (mg/L)	Actual removal (%)	Predicted removal (%)
1	7.00	8.00	0.60	35.00	76.10	76.70
2	7.00	8.00	0.60	35.00	76.90	76.70
3	7.00	8.00	1.00	35.00	85.80	85.80
4	9.00	10.00	0.80	22.50	87.00	86.70
5	7.00	8.00	0.60	35.00	76.10	76.70
6	9.00	6.00	0.40	47.50	68.10	67.60
7	5.00	10.00	0.80	22.50	82.40	82.32
8	7.00	8.00	0.60	10.00	78.30	78.93
9	9.00	10.00	0.80	47.50	85.10	85.14
10	9.00	10.00	0.40	47.50	73.80	73.61
11	5.00	6.00	0.80	22.50	75.90	76.16
12	9.00	6.00	0.80	22.50	80.70	80.19
13	5.00	6.00	0.40	47.50	60.60	60.98
14	5.00	10.00	0.40	47.50	66.70	66.64
15	9.00	6.00	0.80	47.50	79.60	80.03
16	9.00	10.00	0.40	22.50	77.00	76.62
17	7.00	8.00	0.60	60.00	75.10	74.97
18	5.00	10.00	0.40	22.50	70.80	70.45
19	7.00	8.00	0.60	35.00	76.90	76.70
20	5.00	6.00	0.40	22.50	64.00	63.39
21	7.00	8.00	0.60	35.00	77.30	76.70
22	5.00	6.00	0.80	47.50	75.40	75.20
23	7.00	8.00	0.20	35.00	61.00	61.50
24	7.00	8.00	0.60	35.00	76.90	76.70
25	7.00	12.00	0.60	35.00	81.40	81.88
26	3.00	8.00	0.60	35.00	66.50	66.65
27	7.00	4.00	0.60	35.00	69.70	69.72
28	11.00	8.00	0.60	35.00	77.30	77.65
29	5.00	10.00	0.80	47.50	80.10	79.96
30	9.00	6.00	0.40	22.50	69.00	69.21

$$\text{HA Removal}(\%) = \frac{(C_0 - C_t)}{C_0} \times 100 \quad (1)$$

where C_0 and C_t are the HA concentration in reaction solution before and after conducting experiments, respectively. Also, total organic carbon (TOC) reduction was used to determine mineralization percentage. TOC of the reaction solution was measured by a vario TOC cube (TOC/TNb Analyzer) apparatus. Mineralization efficiency was calculated based on TOC concentration according to Eq. (2).

$$\text{Mineralization efficiency}(\%) = \left(1 - \frac{\text{TOC}_t}{\text{TOC}_0}\right) \times 100 \quad (2)$$

where TOC_0 and TOC_t represent the TOC content of the HA solution before and after conducting the removal experiments, respectively.

3. Results and discussion

3.1. Characterization of the synthesized catalysts

The results related to SEM analysis are depicted in Fig. 2. Figs. 2a and b show the morphology and physical features of the synthesized rGO under magnifications of 75 kV and 200 kx, respectively. As seen, the rGO is formed in a sheeted and wrinkled shape with a relatively large surface area that can be selected as a promising platform and support for the C-MgO. The results are consistent with the previous report [33]. Fig. 2c obviously illustrates that the C-MgO was uniformly loaded and anchored onto the surface of the rGO. The similar results were found in the study of Zhou et al. [38]. The C-MgO decorated onto the surface of the rGO is gray to black in color. It can be attributed to the presence of sucrose during the synthesis and calcination of the MgO to produce the C-MgO. From the image scale, it can be observed that the C-MgO particles onto the rGO surface are extended into nano-sized range.

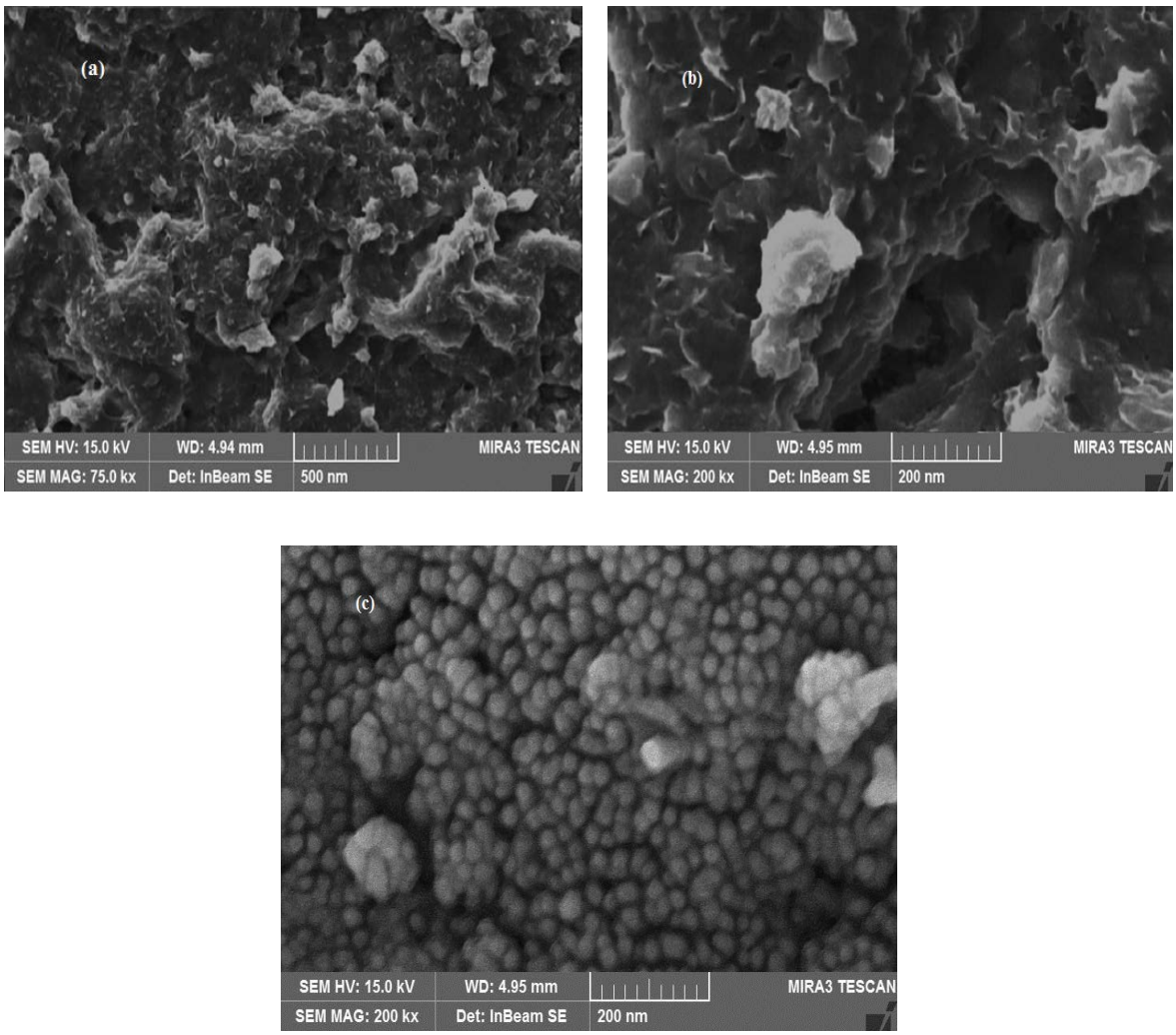

Fig. 2. Scanning electron microscope (SEM) images for rGO (a) and (b), rGO/C-MgO composite (c).

The results of BET analysis based on N_2 adsorption have been demonstrated in Fig. 3a, revealing a specific surface area of around 252 m^2/g for the rGO/C-MgO. Moreover, the total pore volume of 0.129 m^3/g was calculated at $P/P_0 = 0.990$. BJH plot, as depicted in Fig. 3b, has verified that the pore size distribution of the rGO/C-MgO has mostly fallen in the range of mesoporous material (2–50 nm). Smaller-sized pores in mesoporous region reflect the porosity in the nanoflakes, while the larger-sized pores can be attributed to the porosity observed among agglomerated nanoflakes. Finally, the average pore diameter of 3.462 nm was obtained for the rGO/C-MgO composite according to BJH analysis.

EDX analysis (Fig. 4) identified the presence of C, O, and Mg in the rGO/C-MgO composite structure with the amounts of 13.19, 35.17, and 51.65 wt%, respectively, confirming the purity of the composite.

XRD patterns of the GO, rGO, and rGO/C-MgO samples have been depicted in Fig. 5. As can be seen from the XRD pattern of the GO, a strong peak has appeared at $2\theta = 12.17°$, which can be ascribed to the (002) planes of the GO. It indicates that the graphite powder is successfully oxidized into the GO. After chemical reduction of the GO, an amorphous broad peak at around 25° is seen for the rGO sample, proving that oxygen-containing functional groups were reasonably eliminated, and the rGO was synthesized as well. Similar results have been reported elsewhere [39]. The diffraction peak related to the MgO presence in the structure of the rGO/C-MgO composite has been revealed in the 2Θ nearly 42.8° (corresponding to the (2 0 0) planes), which indicates the dominant presence of the MgO in the synthesized composite. According to the Joint Committee on Powder Diffraction Standard (45–0946), these results are in a good agreement with the main peaks of periclase MgO [40]. Meanwhile, the rGO-related peak has almost disappeared, or its intensity has decreased at the XRD pattern of the rGO/C-MgO. It may be due to much stronger diffraction peaks of the C-MgO in comparison with rGO [41].

To further assess the reduction of the GO into rGO and to monitor the degree of reduction, UV-Vis spectra of the GO and rGO samples were taken, and related results have been depicted in Fig. 6. It is found that GO possesses a peak at a wavelength of 232 nm arising from π–π^* transitions of graphitic C–C bonds [42]. Fig. 6 also exhibits that after reduction, the rGO reveals a sharper shifted peak at a wavelength of

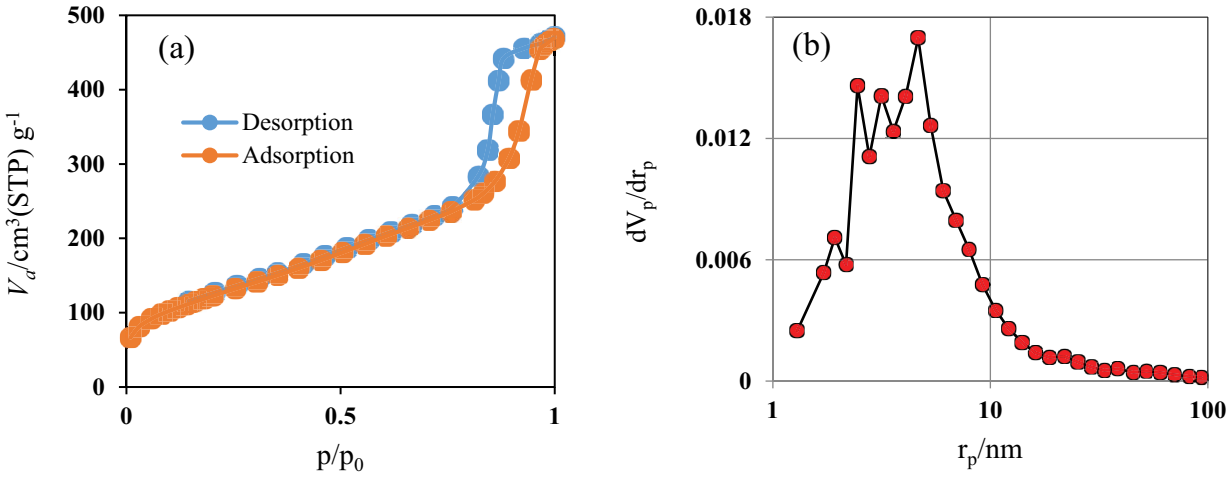

Fig. 3. N_2 adsorption/desorption isotherm (a) and BJH pore size distribution (b) for the rGO/C-MgO.

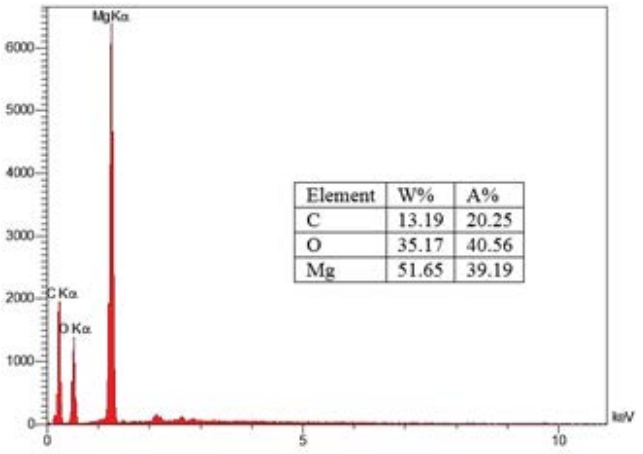

Element	W%	A%
C	13.19	20.25
O	35.17	40.56
Mg	51.65	39.19

Fig. 4. Energy-dispersive X-ray (EDX) analysis for the rGO/C-MgO composite.

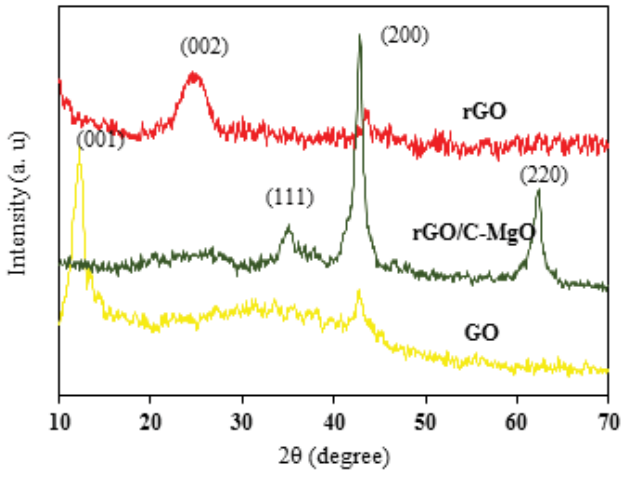

Fig. 5. XRD analysis for the GO, rGO, and rGO/C-MgO composite.

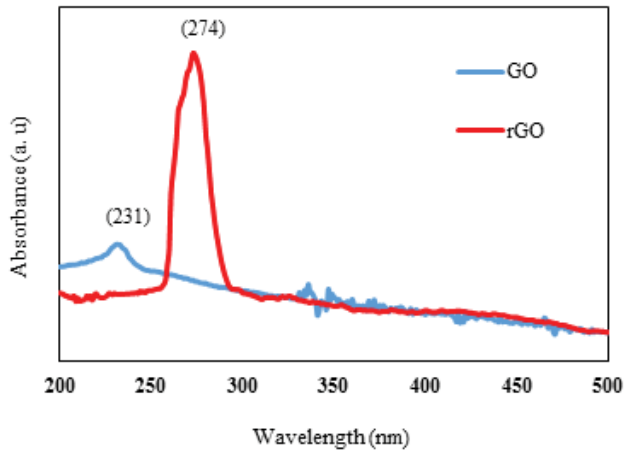

Fig. 6. UV-Vis spectra of the GO and rGO.

274 nm, which is due to π–π* transitions of graphitic C–C ring [42]. Similar findings were found in the work of Li et al. [43].

3.2. Catalytic and adsorbing performance

Fig. 7 exhibits the performance of the single ozonation in the removal of HA and the potential of the synthesized MgO, C-MgO, and rGO to both adsorption and catalytic ozonation of HA. Further, the influence of the three different ratios of the rGO/C-MgO composite on the performance of the catalytic ozonation is observable. The corresponding results demonstrate that removal efficiency of HA reaches to 15.7% in single ozonation. Thus, it can be deduced that ozonation alone results in relatively low removal efficiency of HA. Moussavi et al. [40] reported 28% removal efficiency of catechol from water using single ozonation. The efficiency difference of the process between the current study and the study of Moussavi et al. [40] can be ascribed to different reasons, such as the type of pollutant, ozone flow, operating time, and NaCl presence. Results also revealed that the

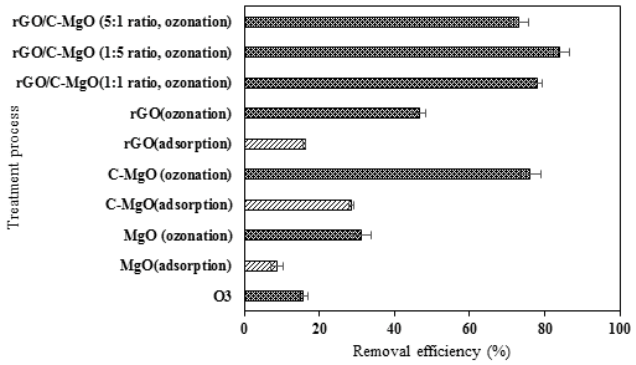

Fig. 7. Catalytic and adsorbing performance of the study processes in the HA removal in the conditions of pH = 9, catalyst dosage = 0.8 g/L, NaCl = 35 mg/L, reaction time = 8 min.

MgO can only adsorb a small quantity (8.6%) of HA from the reaction solution, while removal efficiency increased by 31.3% in the ozonation process catalyzed with the MgO. Therefore, 7% synergistic effect was achieved with the integration of the MgO and ozonation according to Eq. (3).

$$\text{Synergistic effect} = [\text{Catalytic ozonation efficiency} - (\text{Ozonation efficiency} + \text{Adsorption efficiency})] \quad (3)$$

This increase can be attributed to indirect oxidation as a consequence of the production of free oxidizing radicals, such as $OH^{\bullet}$. In general, heterogeneous catalytic ozonation involves two main mechanisms for the degradation of organic contaminants, including indirect and direct oxidation. These mechanisms can occur both on the surface of the catalyst and in the bulk solution, as described in the following reactions [40]:

(I) Indirect reactions

(a) catalyst surface reaction

$$MgO^{OH^{\bullet}} + \text{humic acid} \rightarrow MgO + CO_2 + H_2O + \text{Intermediates} \quad (4)$$

$$MgO^{-\text{humic acid}} + OH^{\bullet} \rightarrow MgO + CO_2 + H_2O + \text{Intermediates} \quad (5)$$

(b) Bulk solution reaction

$$OH^{\bullet} + \text{humic acid} \rightarrow CO_2 + H_2O + \text{Intermediates} \quad (6)$$

(II) Direct (molecular O_3) reactions
(a) Catalyst surface reaction:

$$MgO^{\bullet O_3} + \text{humic acid} \rightarrow MgO + CO_2 + H_2O + \text{Intermediates} \quad (7)$$

$$MgO^{-\text{humic acid}} + O_3 \rightarrow MgO + CO_2 + H_2O + \text{Intermediates} \quad (8)$$

(b) Bulk solution reaction

$$O_3 + \text{humic acid} \rightarrow CO_2 + H_2O + \text{Intermediates} \quad (9)$$

The results related to comparison of the C-MgO and MgO in HA adsorption revealed that the C-MgO leads to approximately 19.8% increase of removal efficiency as compared with MgO. The increase can be explained by the fact that producing the MgO in the presence of sucrose remarkably decreases the agglomeration intensity of the MgO particles, which subsequently leads to an enhancement of specific surface area value of the C-MgO. In addition, the presence of carbon element into the C-MgO structure can possibly play a key role in increasing the removal efficiency [44]. The synergistic effect of ozonation catalyzed with the C-MgO was calculated as 32%, while that of ozonation catalyzed with the MgO was obtained as 7%. The 25% synergistic difference effect between the two systems may be related to oxygen vacancy defects resulted from the substitution of atoms of O by C in the C-MgO. These defects act as active centers generating $O_2^{\bullet-}$radicals and thus promote catalytic activity of the C-MgO [23]. In some studies, a number of nonmetal elements such as S, C, N were used to enhance oxygen vacancy defect of catalysts [23–25]. The mechanism involved in the creation of oxygen vacancy defect is by replacing O atoms in a MgO lattice with C atoms. The following reactions indicate how the reactive oxygen species, such as $O_2^{\bullet-}$, formed lead to the oxidation of the HA. Eq. (10) shows that dissolved oxygen is adsorbed on the C-MgO.

$$\text{Dissolved } O_2 + C - MgO \rightarrow \left[O_2 \ldots C - MgO\right] \quad (10)$$

Eq. (11) is related to the dissociation of adsorbed oxygen into $O_2^{\bullet-}$.

$$O_2 \ldots C - MgO \rightarrow O_3 \rightarrow [O_2^{\bullet-} \ldots C - MgO^{+}] \quad (11)$$

Eq. (12) exhibits that $O_2^{\bullet-}$ radicals can react with water molecules and consequently produce $OH^{\bullet}$ radicals.

$$[O_2^{\bullet-} \ldots C - MgO^{+}] + 2H_2O \rightarrow [HO^{\bullet} \ldots C - MgO^{+}] + 3OH^{-} \quad (12)$$

To specify the main degradation mechanism of HA in the ozonation process catalyzed with the MgO and C-MgO, salicylic acid, at the given experimental condition in Fig. 8, was applied to scavenge $OH^{\bullet}$ radical, due to its greater reactivity toward $OH^{\bullet}$ (2.2×10^{10} $M^{-1}S^{-1}$) as compared with other scavengers, such as tert-butanol (6×10^{8} $M^{-1}S^{-1}$) and methanol (9×10^{8} $M^{-1}S^{-1}$) [18]. Also, chloroform was used as a scavenger for $O_2^{\bullet-}$ radicals due to its high reactivity toward the radical (3×10^{10} $M^{-1}s^{-1}$) [34]. The corresponding results, as seen in Fig. 8, indicates a large reduction in the HA removal in the catalytic ozonation with the MgO, in the presence of salicylic acid, while the decrease in removal efficiency was found to be much lower for catalytic ozonation with the C-MgO catalyst. It must be noted that, in the presence of chloroform, the efficiency of catalytic ozonation with the C-MgO was dramatically decreased. It can be, therefore, deduced that the MgO has catalyzed the catalytic ozonation process further

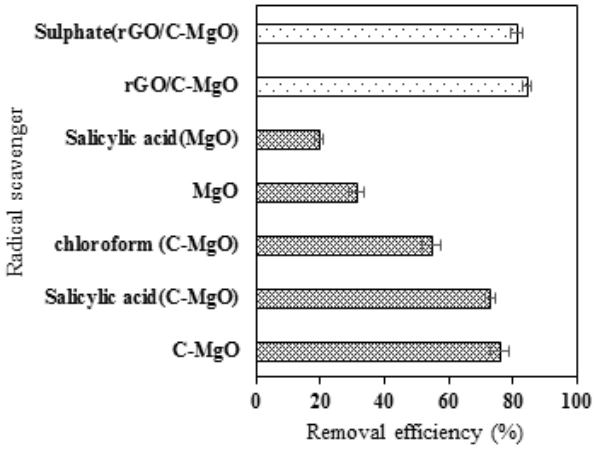

Fig. 8. HA removal efficiency in the catalytic ozonation catalyzed by the MgO and C-MgO in the presence of salicylic acid and by rGO/C-MgO in the presence of sulfate (pH = 9, C-MgO dosage = 0.8 g/L, MgO dosage = 0.8 g/L, reaction time = 8 min, salicylic acid = 0.1 g/L, sulfate = 0.1 g/L NaCl = 35 mg/L).

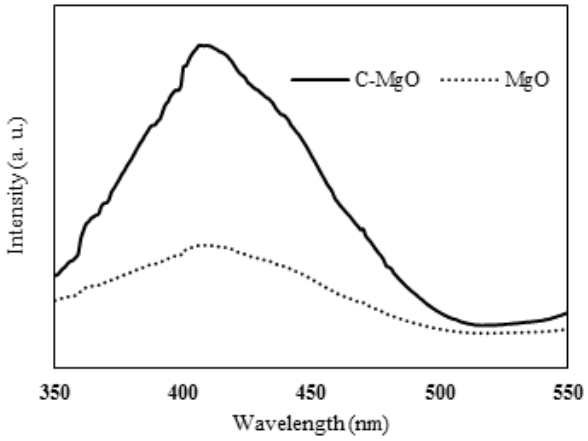

Fig. 9. Photoluminescence spectra for the MgO and C-MgO.

through $OH^{\bullet}$ radicals because using the salicylic acid efficiently reduced the removal efficiency in the system. On the other hand, a slight reduction of removal efficiency in the catalytic ozonation with the C-MgO in the presence of salicylic acid, and on the contrary, a great reduction of that in the system in the presence of chloroform confirmed that non-hydroxyl radicals such as $O_2^{\bullet-}$ may be the most responsible agents in the removal of HA in the catalytic ozonation with the C-MgO. Therefore, it can be concluded that the oxygen vacancy defects appropriately have occurred into the C-MgO structure, which subsequently lead to the increased formation of reactive oxygen species such as $O_2^{\bullet-}$. In the study of Moussavi et al. [23], S element was used to increase the number of oxygen vacancy defects in the MgO structure. They reported that the efficiency of catalytic ozonation of antibiotic tetracycline is more increased in the presence of S-MgO in comparison with MgO [23]. In the studies of Wu et al. [25] and Qin et al. [45], C element was served for forming oxygen vacancy defect into TiO_2 structure.

In the following, to further assess the increased presence of oxygen vacancy sites into the C-MgO structure relative to the MgO, PL analysis was performed. As displayed in Fig. 9, a strong peak at about 420 nm has appeared in the wavelength range of 350–550 nm for the C-MgO, while it has appeared in lower intensity for the MgO. This result verifies an increase in oxygen vacancy sites resulted from the presence of C element in the C-MgO structure. Fig. 7 also shows the effect of the use of the rGO in catalytic ozonation. It was observed that the application of the rGO as a catalyst in catalytic ozonation leads to a 14.9% increase of removal efficiency as compared with the sum of removal efficiencies obtained from single adsorption and ozonation processes. The efficiency increase is originated from the synergistic effect achieved from hybrid rGO-catalyzed ozonation. The synergistic effect may arise from further exposure of the pollutant to ozone molecules (direct oxidation) through enriching the HA molecules around the rGO surface, and from increased catalytic reactions (indirect oxidation) because of electron transfer by the rGO into catalytic ozonation [28]. Fig. 7 also shows that use of the rGO/C-MgO at the rGO to C-MgO ratio of 1:5 (w/w) leads to an 8% increase of synergistic effect than the application of the C-MgO in catalytic ozonation. It can be explained in this way that the rGO by adsorbing the HA onto the surface of rGO/C-MgO, in addition to the positive effect on direct oxidation, make it more probable to collide HA and oxidizing radicals together. This occurrence helps indirect oxidation appear more efficient. Additionally, as addressed above, increased electron transfer is the other route that the rGO can help improve the efficiency removal via indirect catalytic oxidation mechanism.

In practical, various anions exist in different water bodies that may negatively affect catalytic ozonation processes. Sulfate, an anion with a relatively high affinity toward active sites of Lewis catalysts and deactivation of those, was utilized to evaluate its effectiveness as an inhibitor [19]. The related results in Fig. 8 show not significantly dropping in the removal efficiency at the presence of the anion. These results reveal the high ability of the rGO/C-MgO to keep its activity in the presence of sulfate anions in the reaction solution. Finally, according to the findings, it can be concluded that non-hydroxyl radical reactions are the main mechanism involved in catalytic ozonation with rGO/C-MgO catalyst for degrading HA from the reaction solution. It is worth noting here that the rGO/C-MgO with 1:5 ratio was the selected catalyst to catalyze catalytic ozonation in the rest of the experiments.

3.3. Statistical analysis and model fitting

The experimental and predicted removal efficiencies of HA by the catalytic ozonation with rGO/C-MgO are given in Table 2. As seen in Table 3, ANOVA results suggested that quadratic polynomial model has the highest correlation with the experimental data (F-value = 363.38 and R-squared (R^2) = 0.9971). The R^2 value expresses that the regression model can predict over 99% of the response variability. Moreover, another evidence of the good fitness of the model to the experimental results is the adjusted R^2 value of 0.9943, very close to the R^2 value. Table 3 also shows that most of

Table 3
ANOVA results of CCD-RSM model for the catalytic ozonation process with the rGO/C-MgO

Factor	Sum of squares	F value	*p*-Value
Model	1,369.90	363.38	<0.0001
pH-A	181.50	674.03	<0.0001
Time-B	222.04	824.58	<0.0001
rGO/C-MgO-C	885.74	3,289.30	<0.0001
NaCl concentration-D	23.60	87.65	<0.0001
AB	0.12	0.45	0.5103
AC	3.24	12.03	0.0034
AD	0.64	2.38	0.1440
BC	0.81	3.01	0.1033
BD	1.96	7.28	0.0165
CD	2.10	7.81	0.0136
A^2	35.49	131.80	<0.0001
B^2	1.39	5.16	0.0383
C^2	15.95	59.22	<0.0001
D^2	0.11	0.40	0.5377
Residual	4.04		
Lack of fit	2.84	1.18	0.4523
R-Squared	Adj R-squared		Pred R-squared
0.9971	0.9943		0.9868

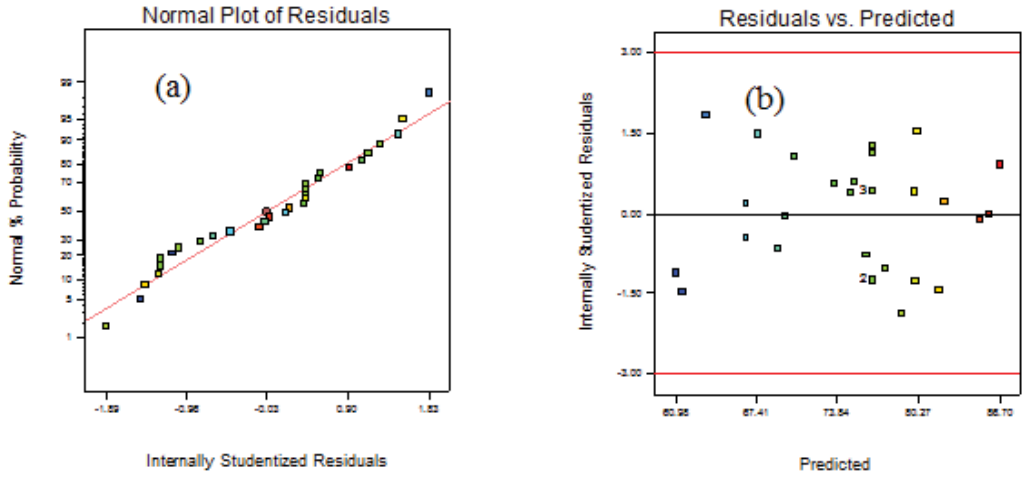

Fig. 10. Normal plot of residuals (a) and the diagnostic plot of residuals vs. predicted values (b).

the linear and square terms included to the model are significant at a *p*-value less than 0.05, while interaction effects were found to be significant for pH × catalyst dosage, time × NaCl concentration and catalyst dosage × NaCl concentration at *p*-value < 0.05.

The assessment of the model adequacy was also performed by means of the normal plot of residuals and residuals vs. predicted plot. The residuals were observed to have a normal distribution as observed in Fig. 10a, where almost all the residuals have fallen on or near the normality line. Also, Fig. 10b indicated that the distribution of residuals vs. predicted values are approximately symmetrical around the zero lines and does not follow a specific trend. Both the plots validate the model adequacy for predicting the values close to actual values.

According to the regression analysis of the results, an empirical model (Eq. (13)) was provided, which determine the relationship between the response and the independent variables in terms of actual factors.

$$\begin{aligned} R(\%) = {} & 10.438 + 5.576X_1 + 3.095X_2 + 60.55X_3 - \\ & 0.1383X_4 + 0.0218X_1X_2 - 1.125X_1X_3 + \\ & 0.008X_1X_4 - 0.5625X_2X_3 - 0.014X_2X_4 + \\ & 0.145X_3X_4 - 0.2843X_1^2 - 0.0562X_2^2 - \\ & 19.062X_3^2 + 0.0004X_4^2 \end{aligned} \quad (13)$$

According to Eq. (14), Pareto effect was calculated for each factor as displayed in Fig. 10.

$$P_i = \left[\frac{(b_i^2)}{\sum b_i^2}\right] \times 100 \quad (14)$$

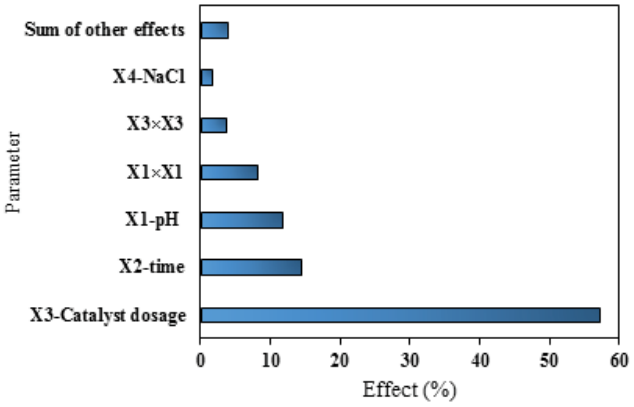

Fig. 11. Pareto chart for determining the effect percentage of each term in the catalytic ozonation with the rGO/C-MgO.

where b represents the regression coefficient of each term in accordance with coded values. As seen in Fig. 11, the contribution of each factor in HA removal using the catalytic ozonation with the rGO/C-MgO is different, and the factors of the catalyst dosage, time and pH were found, respectively, to have the highest effects on the process.

3.4. Optimization of independent variables and effect of the independent variables on the catalytic ozonation with the rGO/C-MgO

The optimization of the independent variables was performed based on the maximum removal efficiency, accordingly, the optimum levels of the variables were obtained at 8.46 of pH, 12 min of reaction time, 1 g/L of catalyst dosage and 10 mg/L of NaCl concentration, as shown in Fig. 12. At these conditions, the maximum removal efficiency obtained was 92.85%. To confirm the ability of the model to predict the removal efficiency close to the actual values, three tests in the proposed optimum levels of variables were examined, and the resulting removal efficiency (92.5% ± 1.97) was found to have no significant difference with the predicted removal efficiency.

The effect of the pH and time parameters on the HA removal efficiency is depicted in Fig. 12a. Fig. 12 generally

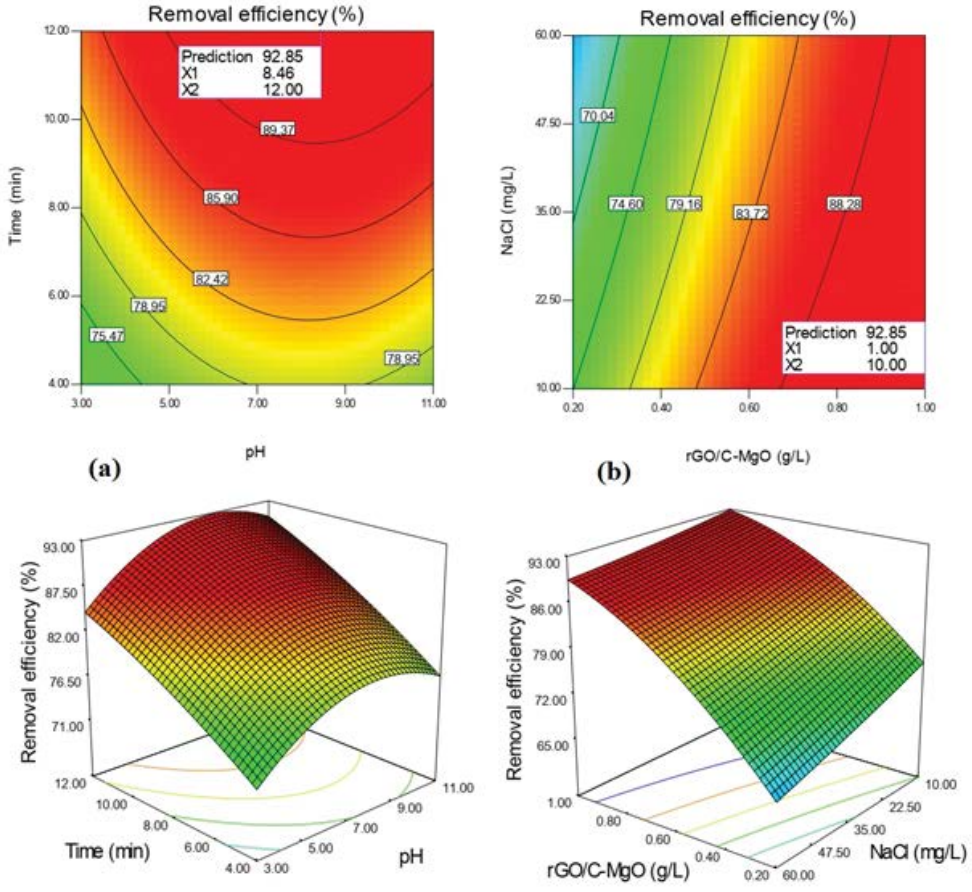

Fig. 12. Optimum levels of the independent parameters in the catalytic ozonation process with rGO/C-MgO, and the effects of pH, time, HA concentration, and rGO/C-MgO dosage on the performance of the catalytic ozonation process.

reveals that the removal efficiency varies from 79.42% in 4 min contact time to 92.85% in 12 min, at the condition of pH = 8.46, catalyst dose = 1 g/L and NaCl = 10 mg/L. Similarly, it increased from about 84.47% to 92.85% by raising pH from 3 to 8.46, at contact time = 12 min, catalyst dose = 1 g/L and NaCl = 10 mg/L. However, a slight decrease at the HA removal was observed at the pHs higher than 9. Overall, in the acidic condition of the solution, the generation of active radicals such as $OH^{\bullet}$ is at lower levels, and dominant mechanism is direct oxidation, while with increasing the pH value of the reaction solution, the produced amount of the oxidizing radicals was elevated, leading to an increase in the HA removal [46]. In terms of HA oxidation reaction in the alkaline condition, ozone was further dissociated to $OH^{\bullet}$ radical, however non-decomposed ozone molecules may play a negligible role in the oxidation, while in acidic, the direct oxidation or directly attacking of ozone molecule to the HA is a prevailing mechanism in HA removal [47]. So, one of the so effective reasons in increasing HA removal in base solution is the presence of hydroxyl (OH^-) ion, which increases the formation of $OH^{\bullet}$. It was previously stated that, in the solution pH greater than pHzpc, the surface of the catalyst is negatively charged because of the OH^- functional group. OH^- ion is known to be the strongest monovalent Lewis base and the catalytic centers of metal oxide [46]. Therefore, Lewis base reaction with O_3 begins the formation of radicals such as the $O_2^{\bullet-}$ and $OH^{\bullet}$ [46]. It seems that the Lewis base reaction on the catalyst surface can be another main reason causing an increase in HA removal in the alkaline condition compared with acidic. The pHzpc of the synthesized catalyst was also determined to better understand the pH effect. As observed in Fig. 13, the pHzpc of the rGO/C-MgO was found to be about 9.4, below which the net charge of the catalyst is positively charged, and above which the net charge is negatively charged. Since the pka (acid dissociation constant) of HA is both around 4 for protonation of carboxylic groups and around 8 for the protonation of phenolate group, so that at the solution pH lower than pka, positive charges become dominant on the rGO/C-MgO surface. As a result, the similar charge of the HA and catalyst at the solution with pHs below pKa of 8 causes an increase in the electrostatic repulsion force and a subsequent decrease in the adsorption rate [22]. The decrease in the HA adsorption by the rGO/C-MgO leads to less exposure of HA to the oxidizing agents involved in the direct and indirect oxidation mechanisms. However, it must be referred to the key role of the oxygen vacancy defect in improving the catalytic ozonation performance, because in the acidic or neutral pHs with a low formation rate of $OH^{\bullet}$ radicals, the sites with the oxygen vacancy defect prevent from the noticeable decrease of HA removal through producing the reactive oxygen species of $O_2^{\bullet-}$.

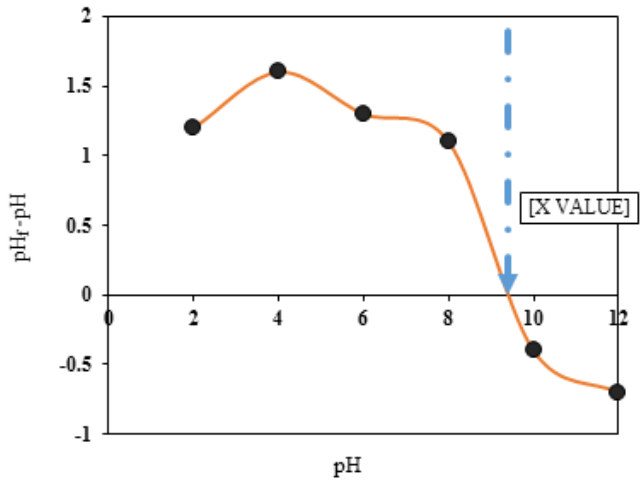

Fig. 13. pH of zero point charge of rGO/C-MgO.

The results revealed higher removal efficiencies in the longer contact times. The reason for the increase is that at a longer contact time, it is more likely that the pollutant collides with oxidizing agents, and a greater opportunity is provided to oxidize and adsorb the pollutant, thereby a higher removal efficiency will be achieved. On the other hand, HA removal rate at the longer contact time was increased with a slower kinetic rate in comparison with that at the earlier contact time. It may be resulted from the reduction of the residual HA amounts in the bulk solution at the higher contact time, which lead to a reduction in the mass transfer rate. The result was consistent with the study of Wang et al. [28] which evaluated the catalytic ozonation with rGO for p-hydroxyl benzoic acid destruction. Moreover, to better explain the effect of reaction time parameter on the performance of the catalytic ozonation with the rGO/C-MgO, the kinetic study of HA removal at the catalyst dosage range from 0.2 to 1 g/L was performed based on the Langmuir–Hinshelwood model as expressed by Eq. (15).

$$\frac{dC_{HA}}{dt} = -k[C_{HA}]\left[C_{Catalyst}\right] \tag{15}$$

Eq. (15) was reduced to Eq. (16) defining a new reaction rate constant of k_{app} instead of $k_{Ccatalyst}$ by assuming pseudo-first-order kinetics [48]. This assumption is from the fact that the selected catalyst dosage is high, with a constant concentration during the kinetic tests

$$\frac{d\left[HA\right]}{dt} = -k_{app}C_{HA} \tag{16}$$

Therefore, the kinetic study of HA removal in the catalytic ozonation was evaluated via fitting the experimental results with Eq. (17), the linearized form of Eq. (16), and the kinetic

Table 4
Pseudo-first-order kinetic model parameters for HA removal by the rGO/C-MgO-catalyzed ozonation at the different dosages of the catalyst

Catalyst dosage (g/L)	Pseudo first-order kinetic information (rGO/C-MgO)		
	K (min^{-1})	R^2	$K_{rGO/C-MgO}$ (min^{-1})
1	0.2092	0.9109	0.1284
0.8	0.1890	0.9209	
0.6	0.1605	0.8968	
0.4	0.1318	0.8912	
0.2	0.1104	0.9097	

information was summarized in Table 3. The high R^2 value of the kinetic model obtained by plotting ln (C_t/C_0) vs. reaction time illustrates that the behavior of HA removal in the catalytic ozonation is described as well by pseudo-first-order kinetics.

$$\ln\frac{C_{\mathrm{HA}t}}{C_{\mathrm{HA}t=0}} = -k_{\mathrm{app}}t \tag{17}$$

The effect of the catalyst dosage and NaCl concentration on the performance of the catalytic ozonation with the rGO/C-MgO is displayed in Fig. 12b. As seen, the removal efficiency of HA has demonstrated a significant increase with increasing the catalyst dose, while it showed a relatively significant reduction with increasing the NaCl concentration. By increasing the catalyst dosage and subsequently the available surface, an increase in the formation of radicals and adsorption rate will occur under constant initial concentration of HA. Accordingly, the elevation in the ratio of the catalyst to HA causes enlarging the removal efficiency [4]. Since salty waters might affect the performance of catalytic ozonation processes, the effect of the presence of NaCl in the synthetic solution was evaluated. As stated earlier, an increase in NaCl concentration had a negative effect but not impressive on the performance of the system. HA removal reached to 89.56% in 60 mg/L NaCl concentration and 92.54% in 10 mg/L at the condition of pH = 8.46, reaction time = 10 min and catalyst dose = 1 g/L. This result was in good agreement with the study of Moussavi et al. [40], in which it was found that the presence of NaCl and HCO_3^- not had a great effect on the performance of catalytic ozonation with MgO/GAC composite.

3.5. Synergistic effect in the optimum operational condition

On the optimum levels of the studied variables, the synergistic effect of the catalytic ozonation with the rGO/C-MgO in HA removal was calculated according to Eq. (2). The synergistic effect of the process was determined to be about 56% (Fig. 14). It exhibits an excellent performance of the combined system of ozonation and the rGO/C-MgO catalyst in the catalytic ozonation process.

Moreover, the degradation capacity and efficiency and removal capacities were determined according to Eqs. (18)–(20)

$$\text{HA removal capacity}\left(\text{mg/g}\right) = \left[\frac{(C_b - C_a)}{C_c}\right]\times 100 \tag{18}$$

$$\text{HA degradation efficiency}\left(\%\right) = \left[\frac{(C_b - C_a) - C_d}{C_b - C_a}\right]\times 100 \tag{19}$$

$$\text{HA degradation capacity}\left(\text{mg/g}\right) = \left[\frac{(C_b - C_a) - C_d}{C_c}\right]\times 100 \tag{20}$$

where C_c denotes the concentration of the rGO/C-MgO, C_b and C_a are the concentration of HA in the beginning and end of the experiments of the catalytic ozonation, respectively, and C_d represents the concentration of HA in the treated solution.

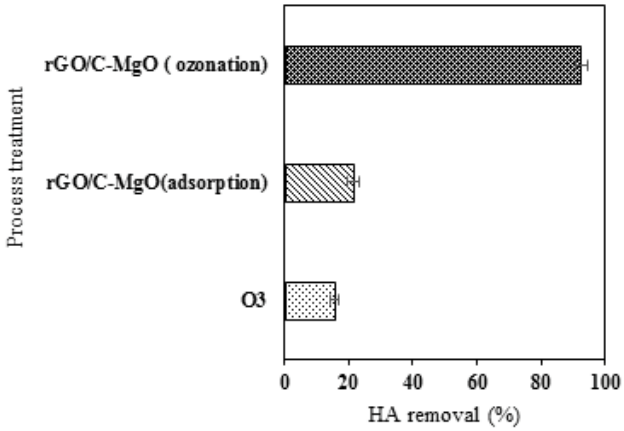

Fig. 14. Comparison of HA removal in the separate and combined agents of the catalytic ozonation process with the rGO/C-MgO (pH = 8.5, reaction time = 12 min, catalyst dose = 1 g/L and NaCl = 10 mg/L).

The results demonstrated removal capacity of 27.85 mg/g, degradation efficiency of 77% and degradation capacity of 21.43 mg/g in the optimum condition of the catalytic ozonation. The destruction efficiency refers to the portion of HA removal by the catalytic ozonation that is the result of oxidation reactions, no adsorption process. The removal capacity represents that 1 g of the rGO/C-MgO is required to remove 27.85 mg of HA, and destruction capacity illustrates that 1 g of rGO/C-MgO must be used to degrade 21.43 mg of HA.

3.6. Mineralization of HA

In the present study, the mineralization degree of HA solution was measured using TOC parameter at the optimum condition of the studied variables. Fig. 15 represents an 86.8% reduction of TOC at 100 min reaction time. At reaction times above 80 min, no noticeable change in TOC removal was observed. This can be ascribed to the production of intermediates with difficult mineralization potential during the degradation reactions [49]. It is worth noting that at 10 min reaction time that is close to the optimum reaction time (12 min), 25.3% reduction of TOC was only obtained.

3.7. Catalytic reusability of rGO/C-MgO

The recyclability of a catalyst is of great importance from the practical and economic point of view; therefore, the current study investigated the reusability of the synthesized rGO/C-MgO in the catalytic ozonation system. After each cycle, the catalyst was recovered by centrifugation, washed with ethanol and water and used in reusability tests after being dried. As observed in Fig. 16, the rGO/C-MgO composite has high stability after five cycles of application in the catalytic ozonation; the removal efficiency of 92.5% in the first use was dropped to 83.9% at the fifth use, as a result, the removal efficiency stayed above 80% after five times of reuse. These results prove the outstanding durability and reusability of the rGO/C-MgO composite for application in the catalytic ozonation process. On the other hand, little

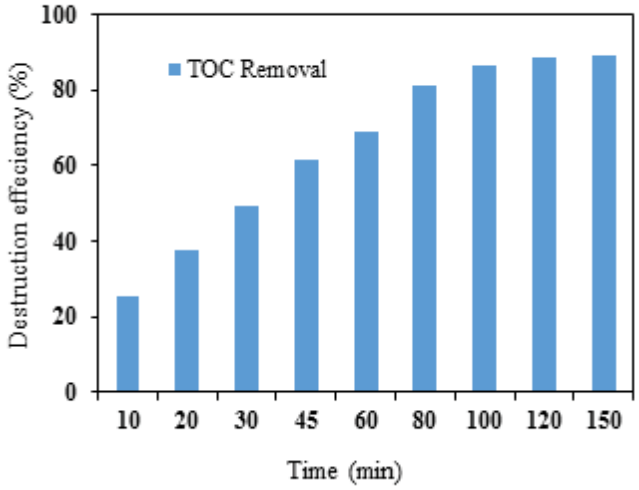

Fig. 15. TOC removal of HA solution in the catalytic ozonation with the rGO/C-MgO (pH = 8.5; catalyst dosage = 1 g/L, NaCl = 10 mg/L).

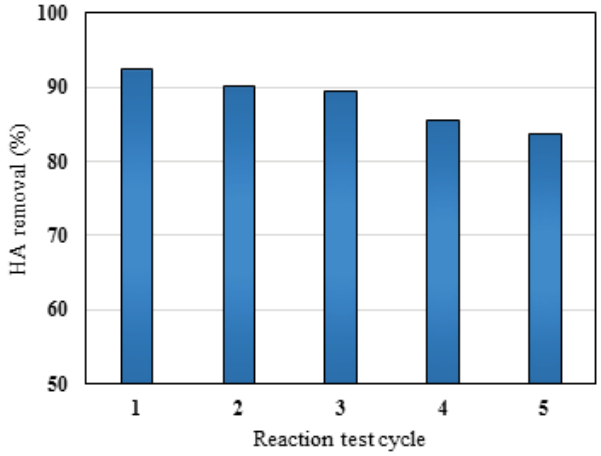

Fig. 16. Reusability of the rGO/C-MgO in the catalytic ozonation for removal of HA (pH = 8.5, reaction time = 12 min, catalyst dosage = 1 g/L and NaCl = 10 mg/L).

change in the HA removal during five consecutive reuses clearly confirmed that the catalytic reactions have been the main mechanism involved in the process, instead of the single adsorption process.

4. Conclusions

This work presented the performance of the catalytic ozonation with the rGO/C-MgO in the HA removal. The characterization analysis revealed that the rGO/C-MgO was synthesized as well. Based on ANOVA results, the quadratic polynomial model had the best fit (F-value of 363.38 and R^2 = 0.9971) with the experimental data, predicting the responses highly close to the actual values of HA removal in the catalytic ozonation with the rGO/C-MgO. Pareto analysis revealed the catalyst dosage possesses the highest effect (about 57%) on the catalytic ozonation performance in HA removal. The optimum values of the independent parameters were obtained at pH = 8.46, contact time = 12 min, catalyst dose = 1 g/L and NaCl = 10 mg/L. In kinetic study, the obtained reaction constant rate based on the pseudo-first-order kinetic model was 0.2092 min^{-1} in 1 g/L catalyst dose, and the calculated synergistic effect at the optimum operational condition was about 56%. TOC reduction of 25.3% and 86.8% was achieved in 10 and 100 min reaction time. Finally, it can be concluded that the rGO/C-MgO can be utilized as a promising catalyst in catalytic ozonation processes for treating waters polluted with HA in high concentrations.

Acknowledgment

The study was funded by Hamadan University of Medical Sciences (Grant Number: 9604132301).

References

[1] V. Oskoei, M. Dehghani, S. Nazmara, B. Heibati, M. Asif, I. Tyagi, S. Agarwal, V.K. Gupta, Removal of humic acid from aqueous solution using UV/ZnO nano-photocatalysis and adsorption, J. Mol. Liq., 213 (2016) 374–380.
[2] X. Wang, Z. Wu, Y. Wang, W. Wang, X. Wang, Y. Bu, J. Zhao, Adsorption–photodegradation of humic acid in water by using ZnO coupled TiO_2/bamboo charcoal under visible light irradiation, J. Hazard. Mater., 262 (2013) 16–24.
[3] O. Turkay, H. Inan, A. Dimoglo, Experimental and theoretical study on catalytic ozonation of humic acid by ZnO catalyst, Sep. Sci. Technol., 52 (2017) 778–786.
[4] S. Mortazavi, G. Asgari, S. Hashemian, G. Moussavi, Degradation of humic acids through heterogeneous catalytic ozonation with bone charcoal, React. Kinet. Mech. Cat., 100 (2010) 471–485.
[5] G. Asgari, A.S. Mohammadi, S.B. Mortazavi, B. Ramavandi, Investigation on the pyrolysis of cow bone as a catalyst for ozone aqueous decomposition: kinetic approach, J. Anal. Appl. Pyrol.. 99 (2013) 149–154.
[6] J.T. Jung, W.H. Lee, J.O. Kim, Photodegradation and permeability of conventional photocatalytic reactor and two different submerged membrane photocatalytic reactors for the removal of humic acid in water, Desal. Wat. Treat., 57 (2016) 26765–26772.
[7] M.A. Mohd Yusof, M.N. Abu Seman, N. Hilal, Development of polyamide forward osmosis membrane for humic acid removal, Desal. Wat. Treat., 57 (2016) 29113–29117.
[8] B. Seredyńska-Sobecka, M. Tomaszewska, A.W. Morawski, Removal of humic acids by the ozonation–biofiltration process, Desalination, 198 (2006) 265–273.
[9] P. Jin, J. Song, L. Yang, X. Jin, X.C. Wang, Selective binding behavior of humic acid removal by aluminum coagulation, Environ. Pollut., 233 (2018) 290–298.
[10] J.N. Wang, A.M. Li, Y. Zhou, L. Xu, Study on the influence of humic acid of different molecular weight on basic ion exchange resin's adsorption capacity, Chin. Chem. Lett., 20 (2009) 1478–1482.
[11] C. An, S. Yang, G. Huang, S. Zhao, P. Zhang, Y. Yao, Removal of sulfonated humic acid from aqueous phase by modified coal fly ash waste: equilibrium and kinetic adsorption studies, Fuel, 165 (2016) 264–271.
[12] G.G. Bessegato, J.C. Cardoso, B.F. Da Silva, M.V.B. Zanoni, Combination of photoelectrocatalysis and ozonation: a novel and powerful approach applied in Acid Yellow 1 mineralization, Appl. Catal., B, 180 (2016) 161–168.
[13] G. Moussavi, A. Alahabadi, K. Yaghmaeian, Investigating the potential of carbon activated with NH_4Cl for catalyzing the degradation and mineralization of antibiotics in ozonation process, Chem. Eng. Res. Des., 97 (2015) 91–99.

[14] Y. Zeng, X. Lin, F. Li, P. Chen, Q. Kong, G. Liu, W. Lv, Ozonation of ketoprofen with nitrate in aquatic environments: kinetics, pathways, and toxicity, RSC Adv., 8 (2018) 10541–10548.
[15] C.-H. Wu, C.-Y. Kuo, C.-L. Chang, Homogeneous catalytic ozonation of CI Reactive Red 2 by metallic ions in a bubble column reactor, J. Hazard. Mater., 154 (2008) 748–755.
[16] J.-E. Lee, B.-S. Jin, S.-H. Cho, S.-H. Han, O.-S. Joo, K.-D. Jung, Catalytic ozonation of humic acids with Fe/MgO, Korean J. Chem. Eng., 22 (2005) 536–540.
[17] J. Chen, S. Tian, J. Lu, Y. Xiong, Catalytic performance of MgO with different exposed crystal facets towards the ozonation of 4-chlorophenol, Appl. Catal., A, 506 (2015) 118–125.
[18] A. Mashayekh-Salehi, G. Moussavi, K. Yaghmaeian, Preparation, characterization and catalytic activity of a novel mesoporous nanocrystalline MgO nanoparticle for ozonation of acetaminophen as an emerging water contaminant, Chem. Eng. J., 310 (2017) 157–169.
[19] G. Moussavi, R. Khosravi, N.R. Omran, Development of an efficient catalyst from magnetite ore: characterization and catalytic potential in the ozonation of water toxic contaminants, Appl. Catal., A, 445 (2012) 42–49.
[20] G. Moussavi, R. Alizadeh, The integration of ozonation catalyzed with MgO nanocrystals and the biodegradation for the removal of phenol from saline wastewater, Appl. Catal., B, 97 (2010) 160–167.
[21] G. Moussavi, A. Yazdanbakhsh, M. Heidarizad, The removal of formaldehyde from concentrated synthetic wastewater using $O3/MgO/H_2O_2$ process integrated with the biological treatment, J. Hazard. Mater., 171 (2009) 907–913.
[22] G. Asgari, M. Salari, Optimized synthesis of carbon-doped nano-MgO and its performance study in catalyzed ozonation of humic acid in aqueous solutions: Modeling based on response surface methodology, J. Environ. Manage., 239 (2019) 198–210.
[23] G. Moussavi, A. Mashayekh-Salehi, K. Yaghmaeian, A. Mohseni-Bandpei, The catalytic destruction of antibiotic tetracycline by sulfur-doped manganese oxide (S–MgO) nanoparticles, J. Environ. Manage., 210 (2018) 131–138.
[24] P. Wang, P.S. Yap, T.T. Lim, C–N–S tridoped TiO_2 for photocatalytic degradation of tetracycline under visible-light irradiation, Appl. Catal., A, 399 (2011) 252–261.
[25] X. Wu, S. Yin, Q. Dong, C. Guo, H. Li, T. Kimura, T. Sato, Synthesis of high visible light active carbon doped TiO_2 photocatalyst by a facile calcination assisted solvothermal method, Appl. Catal., B, 142–143 (2013) 450–457.
[26] F. Dong, S. Guo, H. Wang, X. Li, Z. Wu, Enhancement of the visible light photocatalytic activity of C-doped TiO_2 nanomaterials prepared by a green synthetic approach, J. Phys. Chem. C, 115 (2011) 13285–13292.
[27] D. Tristantini, E. Kusrini, D. Philo, Simple methods for immobilizing titania into pumice for photodegradation of phenol waste, Int. J. Ind. Chem., 9 (2018) 127–139.
[28] Y. Wang, Y. Xie, H. Sun, J. Xiao, H. Cao, S. Wang, Efficient catalytic ozonation over reduced graphene oxide for p-hydroxylbenzoic acid (PHBA) destruction: active site and mechanism, ACS Appl. Mater. Interfaces, 8 (2016) 9710–9720.
[29] M. Nasrollahzadeh, S.M. Sajadi, A. Rostami-Vartooni, M. Alizadeh, M. Bagherzadeh, Green synthesis of the Pd nanoparticles supported on reduced graphene oxide using barberry fruit extract and its application as a recyclable and heterogeneous catalyst for the reduction of nitroarenes, J. Colloid Interface Sci., 466 (2016) 360–368.
[30] X. Feng, Y. Fan, N. Nomura, K. Kikuchi, L. Wang, W. Jiang, A. Kawasaki, Graphene promoted oxygen vacancies in perovskite for enhanced thermoelectric properties, Carbon, 112 (2017) 169–176.
[31] M. Salari, M.H. Dehghani, A. Azari, M.D. Motevalli, A. Shabanloo, I. Ali, High performance removal of phenol from aqueous solution by magnetic chitosan based on response surface methodology and genetic algorithm, J. Mol. Liq., 285 (2019) 146–157.
[32] B.Y.Z. Hiew, L.Y. Lee, K.C. Lai, S. Gan, S. Thangalazhy-Gopakumar, G.-T. Pan, T.C.-K. Yang, Adsorptive decontamination of diclofenac by three-dimensional graphene-based adsorbent: Response surface methodology, adsorption equilibrium, kinetic and thermodynamic studies, J. Environ. Res., 168 (2019) 241–253.
[33] Y. Xie, M. Sun, Y. Shen, H. Li, G. Lv, Z. Cai, C. Yang, G.A.A. Ali, F. Wang, X. Zhang, Preparation of rGO–mesoporous silica nanosheets as Pickering interfacial catalysts, RSC Adv., 6 (2016) 101808–101817.
[34] U. Farooq, M. Danish, S. Lu, M. Naqvi, X. Gu, X. Fu, X. Zhang, M. Nasir, Synthesis of nZVI@ reduced graphene oxide: an efficient catalyst for degradation of 1, 1, 1-trichloroethane (TCA) in percarbonate system, Res. Chem. Intermed., 43 (2017) 3219–3236.
[35] Y. Hu, S. Song, A. Lopez-Valdivieso, Effects of oxidation on the defect of reduced graphene oxides in graphene preparation, J. Colloid Interface Sci., 450 (2015) 68–73.
[36] M. Heidarizad, S.S. Şengör, Synthesis of graphene oxide/magnesium oxide nanocomposites with high-rate adsorption of methylene blue, J. Mol. Liq., 224 (2016) 607–617.
[37] A. Azari, M. Salari, M.H. Dehghani, M. Alimohammadi, H. Ghaffari, K. Sharafi, N. Shariatifar, M. Baziar, Efficiency of magnitized graphene oxide nanoparticles in removal of 2, 4-dichlorophenol from aqueous solution, J. Mazandaran Univ. Med. Sci., 26 (2017) 265–281.
[38] K. Zhou, L. Li, X. Ma, Y. Mo, R. Chen, H. Li, Activated carbons modified by magnesium oxide as highly efficient sorbents for acetone, RSC Adv., 8 (2018) 2922–2932.
[39] G. Liu, L. Wang, B. Wang, T. Gao, D. Wang, A reduced graphene oxide modified metallic cobalt composite with superior electrochemical performance for supercapacitors, RSC Adv., 5 (2015) 63553–63560.
[40] G. Moussavi, A.A. Aghapour, K. Yaghmaeian, The degradation and mineralization of catechol using ozonation catalyzed with MgO/GAC composite in a fluidized bed reactor, Chem. Eng. J., 249 (2014) 302–310.
[41] S.K. Abdel-Aal, A. Ionov, R. Mozhchil, A.H. Naqvi, Simple synthesis of graphene nanocomposites MgO–rGO and Fe 2 O 3–rGO for multifunctional applications, Appl. Phys. A. 124 (2018) 365.
[42] N. Hidayah, W.-W. Liu, C.-W. Lai, N. Noriman, C.-S. Khe, U. Hashim, H.C. Lee, Eds., Comparison on Graphite, Graphene Oxide and Reduced Graphene Oxide: Synthesis and Characterization, AIP Conference Proceedings, 2017, AIP Publishing.
[43] D. Li, M.B. Müller, S. Gilje, R.B. Kaner, G.G. Wallace, Processable aqueous dispersions of graphene nanosheets, Nat. Nanotechnol., 3 (2008) 101.
[44] Q. Zhou, J.-W. Yang, Y.-Z. Wang, Y.-H. Wu, D.-Z. Wang, Preparation of nano-MgO/Carbon composites from sucrose-assisted synthesis for highly efficient dehydrochlorination process, Mater. Lett., 62 (2008) 1887–1889.
[45] Y.H. Qin, Y. Zhuang, R.L. Lv, T.L. Wang, W.G. Wang, C.W. Wang, Pd nanoparticles anchored on carbon-doped TiO_2 nanocoating support for ethanol electrooxidation in alkaline media, Electrochim. Acta, 154 (2015) 77–82.
[46] B. Kasprzyk-Hordern, M. Ziółek, J. Nawrocki, Catalytic ozonation and methods of enhancing molecular ozone reactions in water treatment, Appl. Catal., B, 46 (2003) 639–669.
[47] J. Nawrocki, B. Kasprzyk-Hordern, The efficiency and mechanisms of catalytic ozonation, Appl. Catal., B, 99 (2010) 27–42.
[48] M.J. Ndolomingo, R. Meijboom, Kinetics of the catalytic oxidation of morin on γ-Al_2O_3 supported gold nanoparticles and determination of gold nanoparticles surface area and sizes by quantitative ligand adsorption, Appl. Catal., B, 199 (2016) 142–154.
[49] M. Moradi, F. Ghanbari, M. Manshouri, K.A. Angali, Photocatalytic degradation of azo dye using nano-ZrO 2/UV/Persulfate: response surface modeling and optimization, Korean J. Chem. Eng., 33 (2016) 539–546.